Massachusetts Institute of Technology
Artificial Intelligence Laboratory

A. I. Memo No. 1046 May 1988

Modeling Robot Flexibility for Endpoint Force Control

Steven D. Eppinger
Warren P. Seering

Abstract

Dynamic models have been developed in an attempt to match the response of a robot arm. The experimental data show rigid-body and five resonant modes. The frequency response and pole-zero arrays for various models of structural flexibility are compared with the data to evaluate the characteristics of the models, and to provide insight into the nature of the flexibility in the robot. Certain models are better able to depict transmission flexibility while others describe types of structural flexibility.

Acknowledgments

This paper describes research done at the Artificial Intelligence Laboratory of the Massachusetts Institute of Technology. Support for the laboratory's artificial intelligence research is provided in part by the System Development Foundation and in part by the Advanced Research Projects Agency of the Department of Defense under Office of Naval Research contract N00014-85-K-0124. Support for this research project is also provided in part by the TRW Foundation.

This research was originally presented in April 1988 at the IEEE International Conference on Robotics and Automation in Philadelphia, Pennsylvania [4].

Copyright ©1988 Massachusetts Institute of Technology

Introduction

Manipulation tasks, such as mechanical assembly and surface following involve interaction between the robot and its environment. In these cases, we feed back the resulting contact forces in hopes of improving performance. Compliant control schemes have been proposed by Raibert and Craig [6], Salisbury [7], Whitney [9], and others. See Whitney's overview [10] for a more complete listing. These methods allow the use of signals from a wrist-mounted force sensor to be used in the closed-loop control of the robot joints.

While the prospect of using the sensed force to improve endpoint force command tracking and to yield better disturbance rejection seems quite reasonable, in practice, closed-loop force control has extremely limited bandwidth. Since it is the use of the sensed force information that gives rise to the stability problems in an otherwise stable system, we should investigate the differences between joint position control and endpoint force control.

Joint position control involves joint position commands and measured joint position feedback. The closed-loop bandwidth is generally limited only to the open-loop crossover of the modeled system. Specifically, the performance can be predicted by modeling the compensator, actuator, and rigid links. (An example of such a model is presented here in the section entitled "Rigid-Body Dynamics".) With the joint feedback at the actuator itself, the unmodeled dynamics in the transmission and links become less important.

Endpoint force control, on the other hand, involves joint force commands and measured endpoint force feedback. The closed-loop bandwidth is generally only a small fraction of the open-loop crossover of the modeled system. In fact, measured performance does not approach that predicted by modeling the compensator, actuator, and rigid links. Since the force feedback is now at the endpoint rather than at the actuator, the unmodeled dynamics in the transmission and links become vitally important.

A good model demonstrates the difference between joint position control and endpoint force control. Previous work [3] has shown the effects of limited actuator bandwidth and of structural flexibility. The term *colocated* control is used to describe the joint position control scheme above, since the sensors used for feedback are located at the same points on the flexible structure as the actuators used. In the endpoint force control scheme, however, the sensors are at the robot tip, while the actuators are at the joints. The sensors are separated from the actuators by flexible transmissions and flexible links. This is termed *noncolocated* control [5].

The goal of this research is to develop suitable models of robot flexibility, with the aim of better understanding the causes of instability and improving the closed-loop bandwidth of endpoint force control. A series of lumped-mass models was previously developed [2] to show that robot flexibility

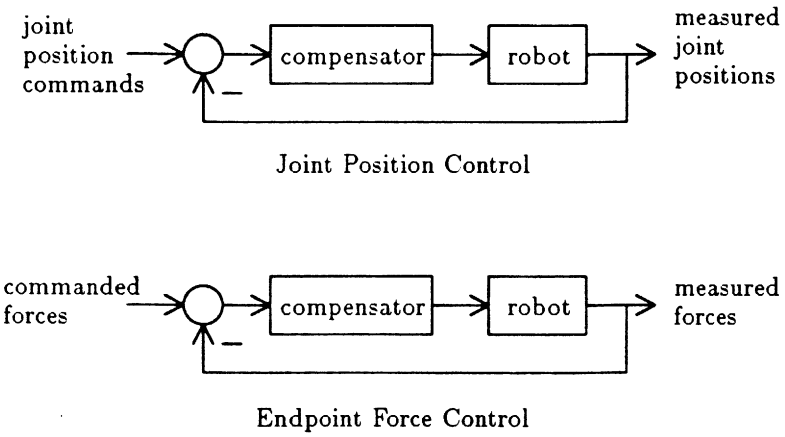

Figure 1: Robot Joint Position Control and Endpoint Force Control

gives rise to force control stability problems, since this is a noncolocated scheme. However, lumped-mass models are not always appropriate, as will be shown here. This paper begins with some experimental robot frequency response data. The limitation of rigid-body models is shown, and then various models of structural flexibility are investigated. Finally, it is concluded that each of the models may be useful to depict the dynamics of a certain type of robot flexibility, and just which model is best for a given robot depends upon the nature of the flexible elements involved.

Experimental Robot Dynamics

As an example to consider throughout this paper, we will consider the dynamics of the MIT Cartesian Assembly Robot, designed and built at the MIT Artificial Intelligence Laboratory. The cartesian gantry-type structure is typical of a large class of robots. While this configuration is different from that of jointed arms, the models developed here may be applied to both types.

The experiment conducted to determine the frequency response of one of the axes is shown in Figure 2. The hardware used includes: a Hewlett-Packard structural dynamics analyzer; the robot's Automatix amplifier and Aerotech motor; the X-axis of the robot structure; and a Bruel & Kjaer accelerometer and charge amplifier. The open-loop transfer function desired is from the amplifier's velocity command input (which is normally the digital controller's output) to the tip motion. The input given to the amplifier was band-limited white noise generated by the HP analyzer. The output measured was tip acceleration of the robot X-axis tested. The analyzer compares the frequency components of the input and output signals, and calculates a transfer function for plotting.

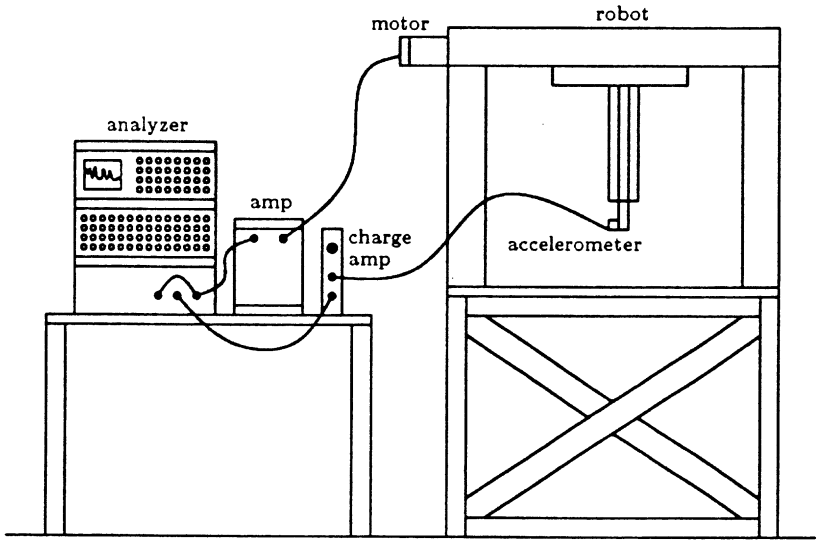

Figure 2: Robot Test Setup

The transfer function for the X-axis is shown in Figure 3 as measured in the experiment described. The dominant structural modes appear to be roughly at 11, 38, 44, 67, and 77 Hz. We would like to develop a dynamic model of this frequency response which can be used in the design of a superior force control scheme.

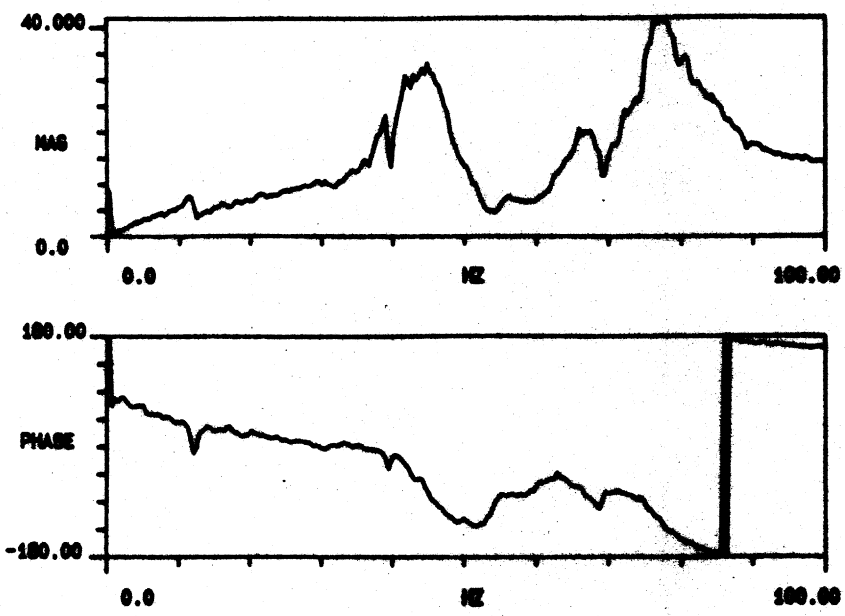

Figure 3: Experimental Transfer Function

Rigid-Body Dynamics

Before attempting to understand the nature of the flexible modes of the robot, we should investigate the theoretical rigid-body behavior. It is this response which limits even the joint position control closed-loop bandwidth. The term *rigid-body* refers to the robot axis modeling only. This model must still include the significant compensator, amplifier, and motor dynamics.

A sketch of the rigid-body dynamic model is shown in Figure 4. The input to this model is the velocity-command voltage given to the preamplifier (this signal usually comes from the digital controller). The preamplifier includes analog tachometer feedback and a gain. The power amplifier is configured as a current (transconductance) amplifier, which is simply a voltage amplifier with sensed current feedback. The power amplifier is actually a pulse-width modulated device with sufficiently high switching frequency that it can be modeled as a linear amplifier. The current feedback comes from the coupled motor model. (Note that modeling the power amplifier simply as a current amplifier would, by causality, force us to ignore the motor dynamics.) The motor input is its terminal voltage. The motor electrical characteristics are constant inductance and resistance, a torque constant, and back EMF. The motor torque output is then proportional to the current. The transmission ratio (ball screw pitch) converts motor torque to force on the axis rigid-body. The robot effective mass to consider here is the total moving mass of the robot, plus the reflected inertias of the rotor and screw. We also include some viscous damping to ground, but no stiffness to ground, since the axis can be positioned anywhere by the actuator. Finally, the rest of the feedback loops are closed, with the velocity again passing through the transmission to get the motor speed.

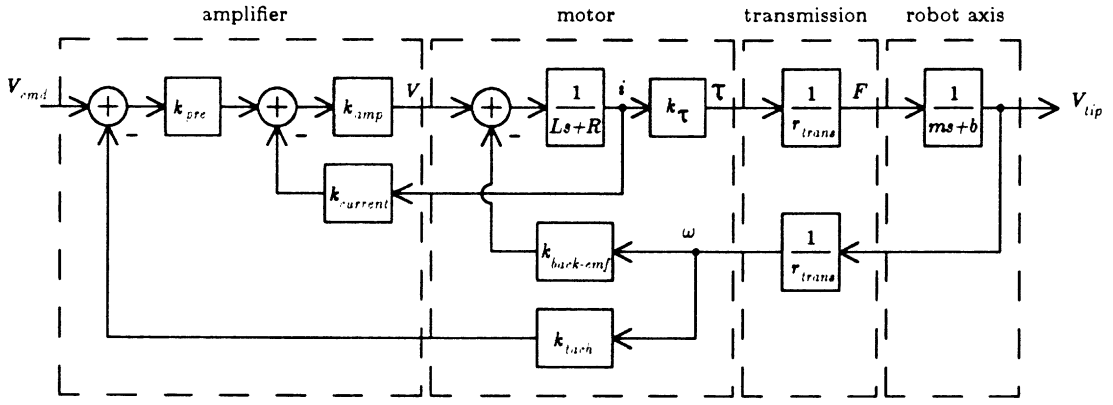

Figure 4: Rigid-Body Robot Model

Along with the flexibility, the many nonlinearities present in the actual system are also neglected in this model. The most significant of these nonlinearities are amplifier saturation and bearing friction. These effects are considered in the simulation used for the controller design.

The transfer function for the linear rigid-body model is then, from amplifier input to tip velocity output:

$$G^v_{rb}(s) = \frac{V_{tip}(s)}{V_{cmd}(s)} = \frac{k_{amp}k_{preamp}r_{trans}k_\tau}{(m_{eff}s+b_{eff})r^2_{trans}(Ls+R+k_{amp}k_{current})+k_\tau(k_{amp}k_{preamp}k_{tach}+k_{back-emf})}$$

We have a second-order transfer function which becomes third order when endpoint position is made the output by adding a free integrator. To compare the frequency response with the experimental data, however, we must add a differentiator instead, to yield tip acceleration, which was measured.

$$G^a_{rb}(s) = sG^v_{rb}(s) = \frac{A_{tip}(s)}{V_{cmd}(s)}$$

The rigid-body model response is shown in Figure 5. We have depicted the overall magnitude and phase response of the robot without its structural dynamics. We now seek a model of the structural resonances.

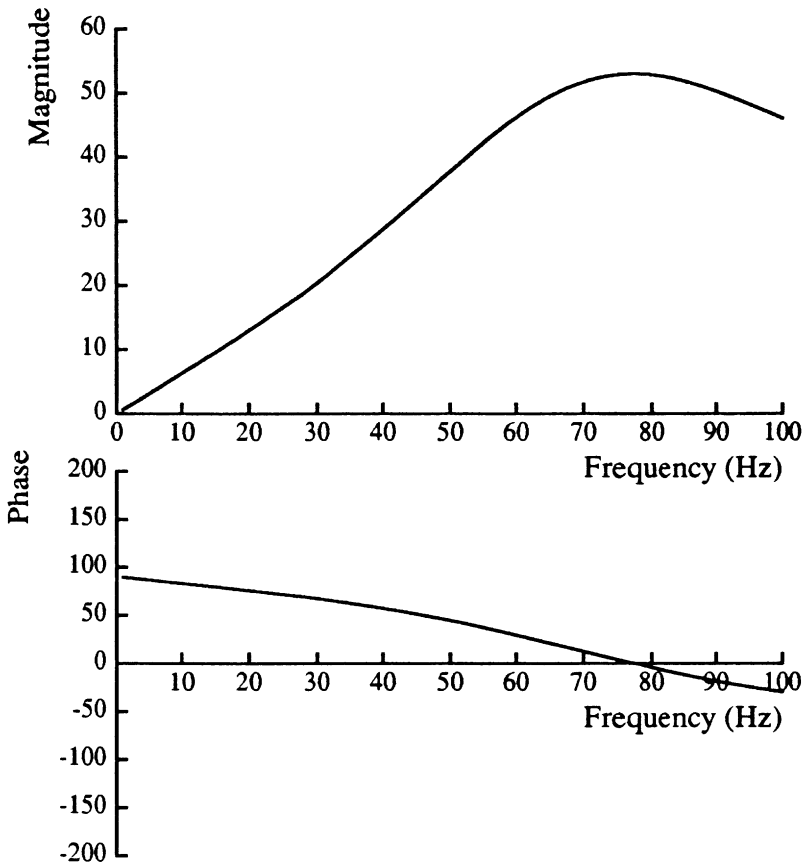

Figure 5: Rigid-Body Model Acceleration

Polynomial Resonance Model

Since the structural resonances are well within the range of interest, we need to model these dynamics also. A simple model of these dynamics can be obtained by constructing a polynomial transfer function to represent the resonances in the transfer function which was obtained by test. The fitted polynomial function, when cascaded with the rigid-body model derived, should match both the magnitude and phase of the experimental transfer function.

We will attempt to match the first five dominant modes in the data. Moreover, we propose to do so by cascading five *simple resonance transfer functions*, each of which has the following form:

$$R_i(s) = \frac{\omega_{pi}^2}{\omega_{zi}^2} \frac{s^2+2\zeta_{zi}\omega_{zi}s+\omega_{zi}^2}{s^2+2\zeta_{pi}\omega_{pi}s+\omega_{pi}^2}$$

Each simple resonance transfer function includes a pair of poles and a pair of zeros only. Each is also scaled to have essentially no effect on the response at $\omega < \min[\omega_{pi}, \omega_{zi}]$.

The overall transfer function that should match the data is then

$$G_p(s) = G_{rb}^a(s)\prod_{i=1}^{5} R_i(s)$$

where $G_{rb}^a(s)$ is the rigid-body model transfer function of tip acceleration output to velocity command input.

The matching of the data takes place as follows:

For each resonance to be matched, starting with the lowest frequency:

1. Compare $|G_p(j\omega)|$ with the experimental transfer function magnitude plot.
2. Find the peak corresponding to the resonance, and set ω_{pi} to the peak frequency.
3. Find the trough corresponding to the resonance, and set ω_{zi} to the trough frequency. (Typically, $\omega_{zi} \approx 1.1\ \omega_{pi}$ for structural modes.)
4. Choose ζ_{pi} to match the height of the peak. (Typically, $\zeta_{pi} \approx .05$ for structural modes.)
5. Choose ζ_{zi} to match the depth of the trough. (Typically, $\zeta_{zi} \approx .05$ for structural modes.)

Note that this method uses the magnitude plots only, and we construct a transfer function to match these. The phase plots should match also, if the data to be matched actually represent a minimum-phase system. Figure 6 shows the frequency response of the polynomial resonance model, which can be compared to the experimental response data in Figure 3.

Since the resonance model is made up by cascading the simple resonance transfer functions with the rigid-body model, its pole-zero array includes the two poles of the rigid-body model, the zero at the

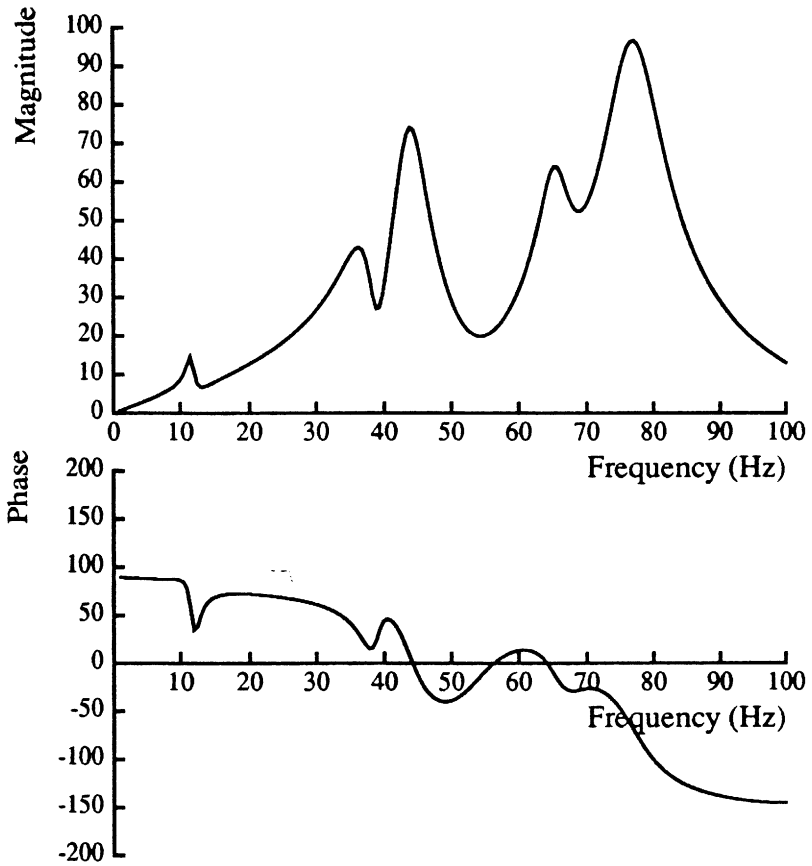

Figure 6: Polynomial Fit to the Experimental Data.

origin which results from choice of acceleration output, and the five pairs of poles and five pairs of zeros of the fitted-polynomial resonance model. This pole-zero array is shown in Figure 7.

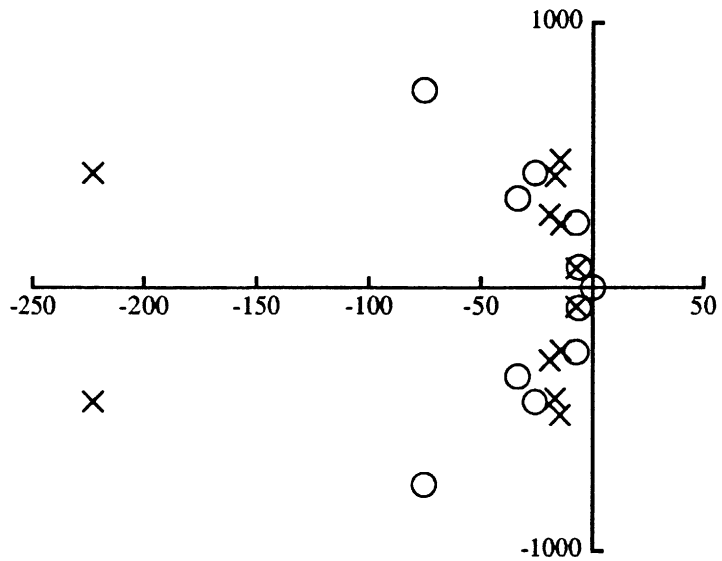

Figure 7: Pole-Zero Array of the Polynomial Resonance Model.

Lumped-Mass Models

The fitted-polynomial resonance model provides an excellent match to the actual system response, however, it lacks the ability to lend physical insight into the behavior exhibited. To improve this situation, we would like to develop a model of the robot structural flexibility which has some physical relevance to the actual hardware.

We first investigate adding flexibility to the rigid-body model discussed earlier. Consider a model of the robot axis which includes flexibility between the actuator and the tip. Figure 8a shows the robot represented by two masses coupled with a spring. This flexible element might depict a transmission compliance or the flexure of a structural element between the actuator and the tip. This configuration attempts to model one mode of vibration in the robot. To depict the first five modes, we would need more vibrating masses.

Consider the substitution of a lumped-mass model, with five springs and six masses in series, Figure 8b, whose resonant frequencies match the first five resonant modes of the robot data. Previous work [2] has analyzed lumped-mass models of this type to show that for each mode of vibration modeled between the actuator and endpoint, two poles are added while only one zero is added in the actuator-to-endpoint transfer function. However, inspection of the experimentally-obtained robot transfer function implies that the correct model of the robot flexibility include two zeros for each pair of poles added. The frequency response of this lumped-mass model cannot possibly match the data, since the transfer function has too few zeros!

We now consider adding the resonant dynamics elsewhere in the lumped-mass model. Specifically, suppose that the actuator and tip are still dynamically colocated on the flexible structure, but there exist flexible elements on the supporting side of the actuator (in the robot base, or frame). Figure 8c shows this configuration. The transfer function from force input to motor (or tip) output velocity now has two zeros and three poles. So two poles and two zeros have now been added to the original rigid-body lumped-mass model by the base dynamics.

This is a plausible model for a class of robot flexibility; however, it results in only colocated transfer functions. That is, it does not address the difference between joint position control and endpoint force control.

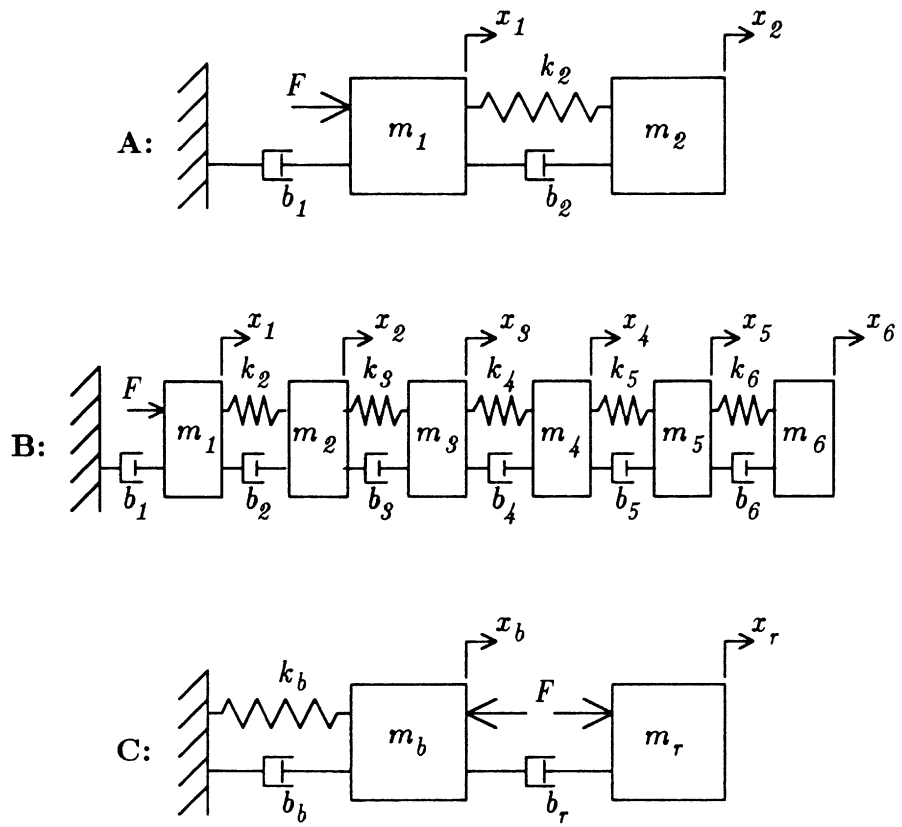

Figure 8: Three Lumped-Mass Models of Robot Axis Flexibility

Bending Beam Models

In search of models of structural flexibility which allow transfer functions to be derived for outputs at various points on the structure, and also allow resonant modes to be added one at a time, we attempt to model a cantilever beam in bending. We model the beam in bending for two reasons: first, the lumped-mass models considered above seem to be discrete models of beams in axial loading (tension/compression), and they failed to properly represent the robot structural modes; and second, the robot structural modes actually look like they are comprised of mostly bending.

Figure 9 shows the distributed-parameter beam robot model. We consider the cantilever beam shown with a sliding constraint at one end and free at the other end. At the sliding end, we apply the actuator force and measure the actuator motion. At the free end, we measure the tip displacement.

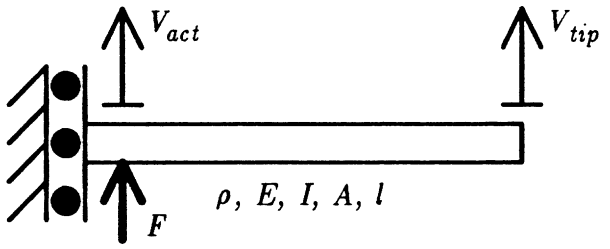

Figure 9: Distributed-Parameter Beam Robot Model

Derivation of equations of motion for such a beam is fairly simple, however, we desire transfer functions. Vaughan [8] has developed a method for the derivation of such transfer functions, although he does not present this particular set of end conditions. Using his procedure, however, we can derive the following relations representing the colocated (actuator) and noncolocated (tip) transfer functions for the sliding-free beam shown.

$$\frac{V_{act}(s)}{F(s)} = \frac{-1}{2}\sqrt{2/p}\,\frac{(S^2+C^2)^2+2S^2+2C^2+1}{(S^2+C^2)^2-4CS-1}$$

$$\frac{V_{tip}(s)}{F(s)} = -2\sqrt{2/p}\,\frac{C(S^2+C^2+1)}{(S^2+C^2)^2-4CS-1}$$

where $S = e^{-\sqrt{Tp}}\sin\sqrt{Tp}$

$C = e^{-\sqrt{Tp}}\cos\sqrt{Tp}$

$p = \frac{s}{a}$

$a^2 = \frac{EI}{\rho A}$

$T = \frac{1}{2}l^2$

and E, I, ρ, A, and l are the beam parameters.

These transfer functions are non-polynomial, and have an infinity of poles and zeros. Nevertheless, we

can plot their frequency response in the normal manner, by substituting $s = j\omega$. Figure 10 shows these frequency response plots, using (Vaughan's) sample beam parameters.

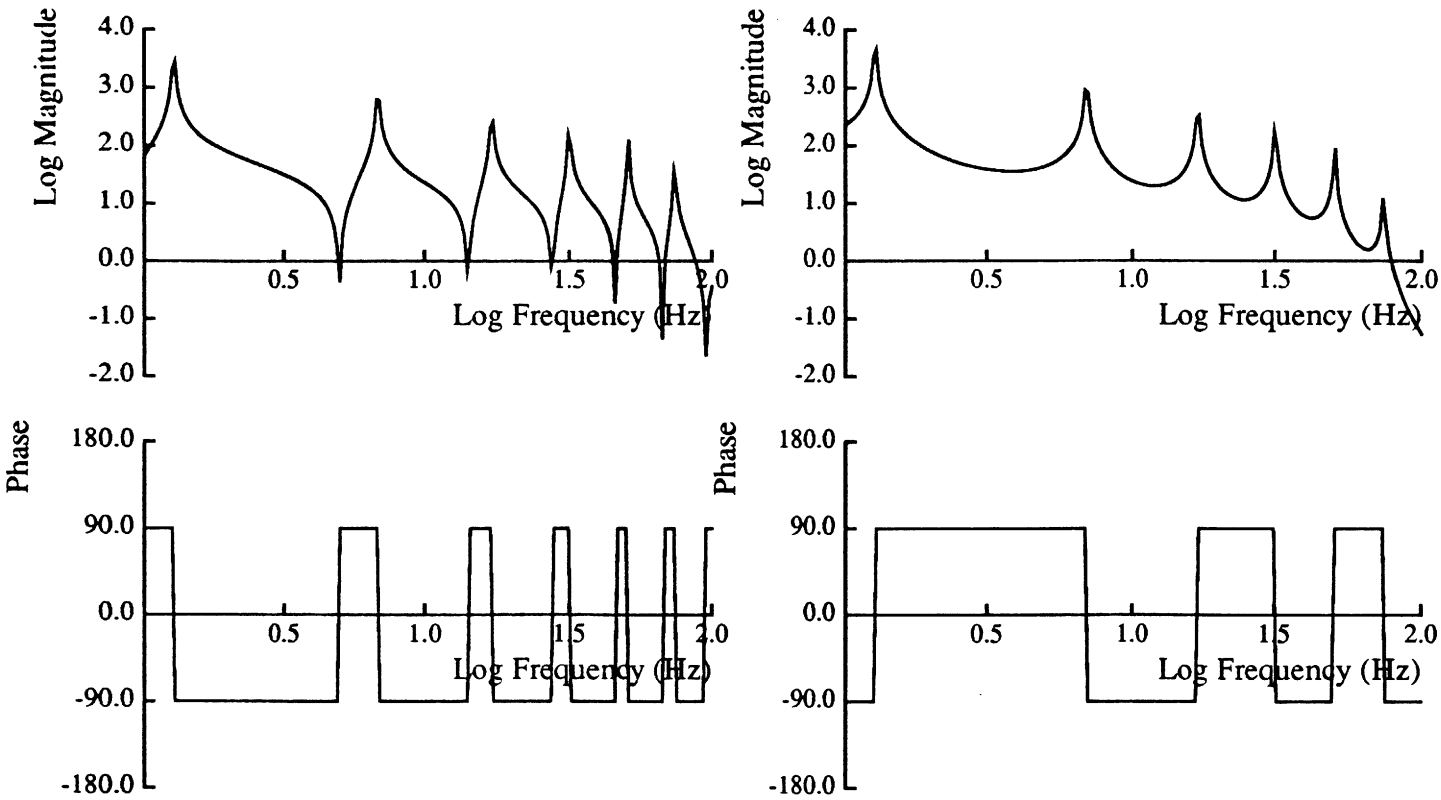

Colocated TF Noncolocated TF

Figure 10: Bode Plots for the Distributed-Parameter Beam Model

Now, to investigate the suitability of this type of beam model to our robot data, we consider the poles and zeros of these transfer functions. While we cannot explicitly solve for the poles and zeros as the roots of the numerator and denominator polynomials of the transfer functions, we can still find the poles and zeros as the points in the s-plane at which the transfer function becomes infinite or zero, respectively. In fact, by doing so, we can construct polynomial approximations to these transfer functions which are valid up to any frequency. Shown in Figure 11 are the pole-zero arrays for the colocated and noncolocated transfer functions of the beam. These polynomial transfer functions match the response of the real beam transfer functions perfectly through the 5^{th} modes. The colocated beam transfer function has poles and zeros in alternating pairs along the $j\omega$ axis. The noncolocated beam transfer function has pairs of poles along the $j\omega$ axis (in the same locations, since the two transfer functions have the same characteristic equation), but the zeros are spread out symmetrically along the positive and negative real axes. The real zeros appear in these "pairs" so as to contribute no net phase shift. (Without these zeros,

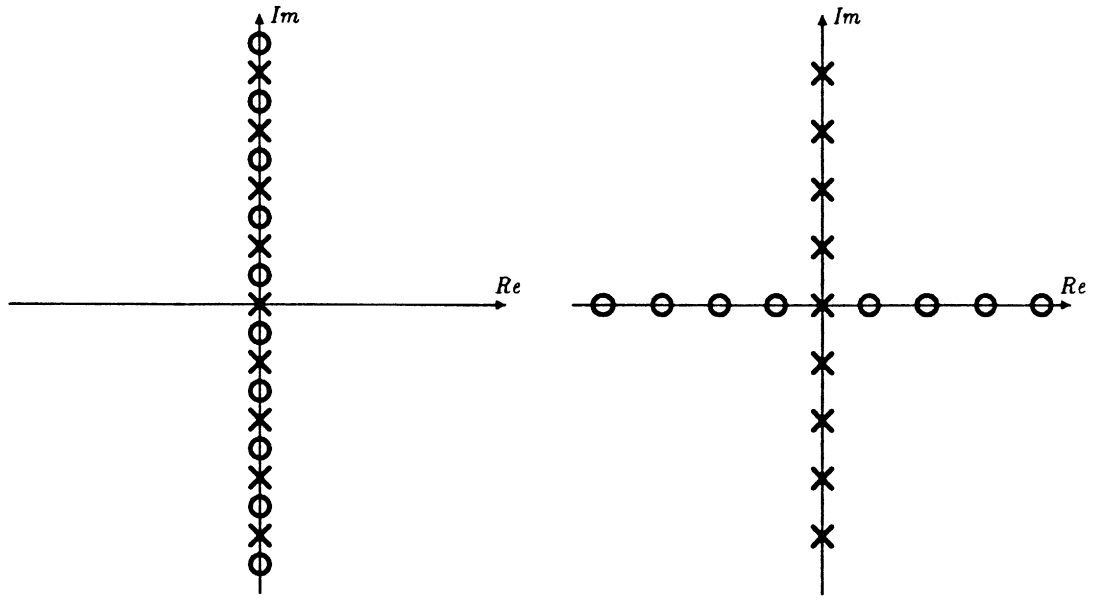

Figure 11: Colocated and Noncolocated Pole-Zero Arrays for the Distributed-Parameter Beam Model

the magnitude response drops off much too fast, and does not match at all.)

The nonminimum phase zeros which appear in the noncolocated transfer function of the distributed-parameter beam robot model are an interesting finding. Similar non-minimum phase properties have been reported by Cannon and Schmitz in their very flexible beam structure [1]. They are curious because they do not appear in any of the lumped-mass models derived above. Is this because the distributed-parameter beam model uses distributed parameters instead of lumped? Or is modeling the bending instead of the tension/compression the significant difference which gives rise to the nonminimum zeros?

We hypothesize that the right-half plane zeros come from the bending effects and not the distributed nature of the model. However, to find out for sure, we derive transfer functions for a lumped-parameter bending-beam model shown in Figure 12. This model is a limited form of the lumped-parameter Timoshenko beam. Here the left-end mass slides, while the right-end mass is free to rotate and translate, as in the distributed-parameter model discussed above.

The equations of motion for this model can be derived and we can solve for the transfer functions from the input force to various outputs. We will describe two such transfer functions, whose pole-zero arrays are shown in Figure 13. The colocated transfer function, from the force input to the position output, x_{act}, is minimum phase. The noncolocated transfer function, from the force input to the position output, x_{tip}, is nonminimum phase. In fact, this noncolocated transfer function also has a "pair" of real zeros at equal frequencies on the positive and negative real axes.

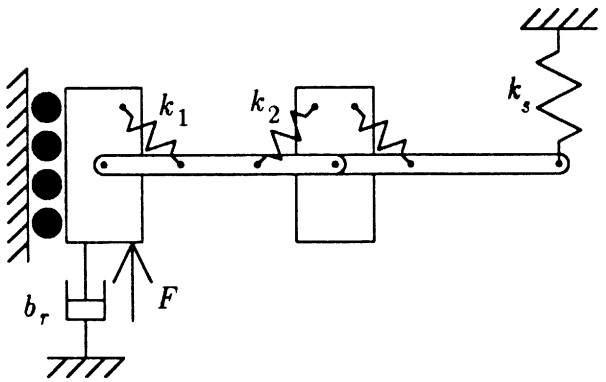

Figure 12: Lumped-Parameter Beam Model

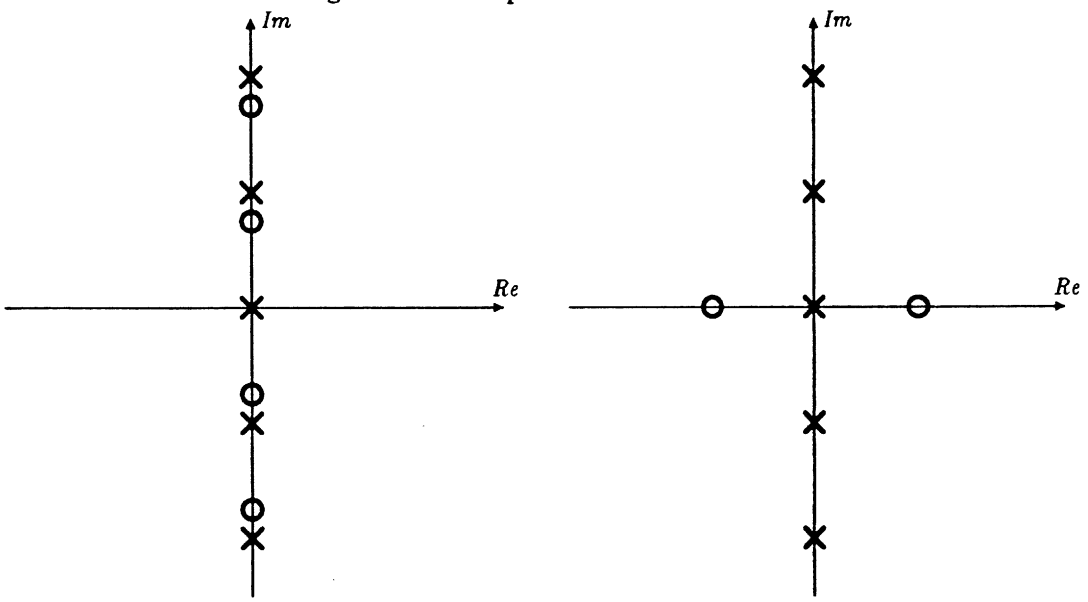

Figure 13: Colocated and Noncolocated Pole-Zero Arrays for the Lumped-Parameter Beam Model

The appearance of the nonminimum phase zeros in the noncolocated transfer functions of both of the bending-beam models again leads us to dismiss these models, since the right-half plane zeros do not appear in the experimental data. The polynomial fit to the experimental data showed pairs of poles and zeros lining up just to the left of the $j\omega$ axis. The distributed-parameter beam model's colocated transfer function has the right numbers of poles and zeros for each mode and the correct arrangement thereof in the s-plane. While this model looks promising, it does not predict any instability for endpoint force control that would not be present for joint position control.

Discussion

We have shown experimental data representing the frequency response of a robot used in our laboratory. We then developed a series of models in an attempt to understand these data.

The **rigid-body robot model** is capable of matching the overall frequency response, with the exception of the resonances. This model considers only the amplifier, motor, and effective rigid-body mass of the arm.

The **polynomial resonance model** matched the robot frequency response quite well, including the first five major resonant modes. This model consists of the rigid-body model, cascaded with two poles and two zeros for each flexible mode. Despite the superior match, this mathematical model bears no physical significance with regard to the actual system.

The **lumped-mass models** have been analyzed previously, and are well understood. When used to depict flexibility between the actuator and tip, these models add for each resonance a pair of poles, and only one zero to the rigid-body model's actuator-to-endpoint transfer functions. When used to describe flexure of the robot base or frame, these models add two zeros with each pair of poles. The former of these configurations is unable to match the data, while the latter lacks the ability to provide both colocated and noncolocated transfer functions.

The **distributed-parameter beam model** showed a striking difference between the pole-zero arrays of its colocated and noncolocated transfer functions. Specifically, the colocated transfer function has poles and zeros alternating along the $j\omega$ axis, while the noncolocated transfer function has the same poles, with its zeros spread out along the positive and negative real axes. The presence of these nonminimum phase zeros explains why at high gain the noncolocated control becomes unstable.

The **lumped-parameter beam model** showed the same nonminimum phase characteristics as its distributed-parameter counterpart. We conclude that the bending modes have significantly different dynamic behavior than axial vibrations in beams.

The two striking observations about these modeling efforts are:

- Only the polynomial resonance model matched the experimental data well. If a high-bandwidth model is required, this method yields an excellent result, although it provides little or no physical insight.
- It is possible for a tip sensor and joint actuator to be *physically noncolocated*, but *dynamically colocated*. That is, while they are separated by flexible elements on the robot structure, for some finite bandwidth, they "move together". The sensor response is equal in phase to the actuator input throughout a given frequency range. Above this bandwidth they

may be *dynamically noncolocated.*

We can divide the sources of robot flexibility into three categories:

1. base flexure
2. transmission compliance
3. link flexure

The transmission compliance is the simplest to model. We would suggest an appropriately chosen lumped-mass model. Base or link flexibility is likely to more closely resemble beam(s) in bending rather than beam(s) in tension or compression, and the lumped masses in series are a discrete approximation to a beam under axial loading. We therefore recommend a beam model for the base or link flexibility. Even a lumped-mass model of a beam in bending displays nonminimum phase zeros at frequencies equal to the minimum phase zeros that appear. Finally, base and link flexure differ significantly in that base flexure allows the joint actuators and tip sensors to remain dynamically colocated, while link flexure may not.

References

[1] Cannon, R.H. and Schmitz, E.
Initial Experiments on the End-Point Control of a Flexible One-Link Robot.
The International Journal of Robotics Research , Fall 1984, vol. 3, no. 3, pp. 62-75.

[2] Eppinger, S.D. and Seering, W.P.
On Dynamic Models of Robot Force Control.
In *Proceedings of International Conference on Robotics and Automation.* IEEE, April 1986, pp. 29-34. Also in *MIT Artificial Intelligence Laboratory Memo*, no. AIM-910).

[3] Eppinger, S.D. and Seering, W.P.
Understanding Bandwidth Limitations in Robot Force Control.
In *Proceedings of International Conference on Robotics and Automation.* IEEE, April 1987, pp. 904-909. Also in *MIT Artificial Intelligence Laboratory Memo*, no. AIM-948).

[4] Eppinger, S.D. and Seering, W.P.
Modeling Robot Flexibility for Endpoint Force Control.
In *Proceedings of International Conference on Robotics and Automation.* IEEE, April 1988, pp. 165-170.

[5] Gevarter, W.B.
Basic Relations for Control of Flexible Vehicles.
AIAA Journal , April 1970, vol. 8, no. 4, pp. 666-672.

[6] Raibert, M.H. and Craig, J.J.
Hybrid Position/Force Control of Manipulators.
In *Journal of Dynamic Systems, Measurement and Control.* ASME, June 1981, vol. 103, no. 2.

[7] Salisbury, J.K.
Active Stiffness Control of a Manipulator in Cartesian Coordinates.
In *Proceedings of 19th Conference on Decision and Control.* IEEE, vol. 1, December 1980.

[8] Vaughan, D.R.
Application of Distributed Parameter Concepts to Dynamic Analysis and Control of Bending Vibrations.
ASME Journal of Basic Engineering , June 1968, pp. 157-166.

[9] Whitney, D.E.
Force Feedback Control of Manipulator Fine Motions.
In *Journal of Dynamic Systems, Measurement and Control.* ASME, June 1977, vol. 99, pp. 91-97.

[10] Whitney, D.E.
Historical Perspective and State of the Art in Robot Force Control.
In *Proceedings of International Conference on Robotics and Automation.* IEEE, March 1985.

CS-TR Scanning Project
Document Control Form

Date : 4/27/98

Report # AIM-1046

Each of the following should be identified by a checkmark:
Originating Department:

☒ Artificial Intellegence Laboratory (AI)
☐ Laboratory for Computer Science (LCS)

Document Type:

☐ Technical Report (TR) ☒ Technical Memo (TM)
☐ Other:_____

Document Information

Number of pages: 18 (23-IMAGES)
Not to include DOD forms, printer instructions, etc... original pages only.

Originals are:
☒ Single-sided or
☐ Double-sided

Intended to be printed as :
☐ Single-sided or
☒ Double-sided

Print type:
☐ Typewriter ☐ Offset Press ☒ Laser Print
☐ InkJet Printer ☐ Unknown ☐ Other:_____

Check each if included with document:

☒ DOD Form ☐ Funding Agent Form ☐ Cover Page
☐ Spine ☐ Printers Notes ☐ Photo negatives
☐ Other: _____

Page Data:

Blank Pages (by page number):_____

Photographs/Tonal Material (by page number):_____

Other (note description/page number):

Description :	Page Number:
IMAGE MAP	(1) UN #'ED TITLE PAGE
	(2-18) PAGES #'ED 1-17
	(19-20) SCANCONTROL, DOD
	(21-23) TRGT 5(3)

Scanning Agent Signoff:
Date Received: 4/27/95 Date Scanned: 5/2/95 Date Returned: 5/4/95

Scanning Agent Signature: Michael W. Cook

UNCLASSIFIED

SECURITY CLASSIFICATION OF THIS PAGE (When Data Entered)

completed 8-26-88

REPORT DOCUMENTATION PAGE

READ INSTRUCTIONS BEFORE COMPLETING FORM

1. REPORT NUMBER: AIM 1046

2. GOVT ACCESSION NO.:

3. RECIPIENT'S CATALOG NUMBER: AD-A195923

4. TITLE (and Subtitle): Modeling Robot Flexibility for Endpoint Force Control

5. TYPE OF REPORT & PERIOD COVERED: memorandum

6. PERFORMING ORG. REPORT NUMBER:

7. AUTHOR(s): Steven D. Eppinger, Warren P. Seering

8. CONTRACT OR GRANT NUMBER(s): N00014-85-K-0124

9. PERFORMING ORGANIZATION NAME AND ADDRESS: Artificial Inteligence Laboratory, 545 Technology Square, Cambridge, MA 02139

10. PROGRAM ELEMENT, PROJECT, TASK AREA & WORK UNIT NUMBERS:

11. CONTROLLING OFFICE NAME AND ADDRESS: Advanced Research Projects Agency, 1400 Wilson Blvd., Arlington, VA 22209

12. REPORT DATE: May 1988

13. NUMBER OF PAGES: 18

14. MONITORING AGENCY NAME & ADDRESS (if different from Controlling Office): Office of Naval Research, Information Systems, Arlington, VA 22217

15. SECURITY CLASS. (of this report):

15a. DECLASSIFICATION/DOWNGRADING SCHEDULE:

16. DISTRIBUTION STATEMENT (of this Report)

Distribution is unlimited.

17. DISTRIBUTION STATEMENT (of the abstract entered in Block 20, if different from Report)

18. SUPPLEMENTARY NOTES

None

19. KEY WORDS (Continue on reverse side if necessary and identify by block number)

robot force control
robot control
robot dynamics
flexible structures

20. ABSTRACT (Continue on reverse side if necessary and identify by block number)

Dynamic models have been developed in an attempt to match the response of a robot arm. The experimental data show rigid-body and five resonant modes. The frequency response and pole-zero arrays for various models of structural flexibility are compared with the data to evaluate the characteristics of the models, and to provide insight into the nature of the flexibility in the robot. Certain models are better able to depict transmission flexibility while others describe types of structural flexibility.

DD FORM 1 JAN 73 1473 EDITION OF 1 NOV 65 IS OBSOLETE
S/N 0102-014-6601

UNCLASSIFIED

SECURITY CLASSIFICATION OF THIS PAGE (When Data Entered)

Scanning Agent Identification Target

Scanning of this document was supported in part by the **Corporation for National Research Initiatives,** using funds from the **Advanced Research Projects Agency** of the **United states Government** under Grant: **MDA972-92-J1029.**

The scanning agent for this project was the **Document Services** department of the **M.I.T Libraries.** Technical support for this project was also provided by the **M.I.T. Laboratory for Computer Sciences.**

Scanned

Date: 5/2/1995

M.I.T. Libraries
Document Services